

Superelastic leg design optimization for an endoscopic capsule with active locomotion

This article has been downloaded from IOPscience. Please scroll down to see the full text article.

2009 Smart Mater. Struct. 18 015001

(<http://iopscience.iop.org/0964-1726/18/1/015001>)

The Table of Contents and more related content is available

Download details:

IP Address: 193.205.81.13

The article was downloaded on 05/01/2009 at 10:10

Please note that terms and conditions apply.

Superelastic leg design optimization for an endoscopic capsule with active locomotion

Elisa Buselli¹, Pietro Valdastrì¹, Marco Quirini¹,
Arianna Menciasci^{1,2} and Paolo Dario^{1,2}

¹ Scuola Superiore Sant'Anna-CRIM Lab, Piazza Martiri della Libertà 33, I-56127 Pisa, Italy

² Istituto Italiano di Tecnologia, Via Morego 30, I-16163 Genova, Italy

Received 31 May 2008, in final form 22 August 2008

Published 28 November 2008

Online at stacks.iop.org/SMS/18/015001

Abstract

Nowadays Nitinol structures are accepted and highly exploited in the medical field. Therefore, studying the mechanical properties of this material—which is not trivial by considering the thermal behaviour of the alloy—is very important in order to get quantitative data for a reliable design of novel Nitinol components. In particular, this study focuses on the design optimization of superelastic Nitinol legs to be integrated into an endoscopic capsule for biomedical applications. The leg is provided with an elastic knee that adds a passive degree of freedom to the structure; this solution allows us to achieve a good locomotion adaptability in the unstructured environment of the gastrointestinal tract, characterized by different diameters. First, the mechanical behaviour of Nitinol was analysed. Tensile tests were carried on in order to extract the peculiar stress–strain curve of the material. The hysteretic behaviour was observed through 100 loading–unloading cycles. The acquired data were used to model the leg design by finite element methods (FEM) and to estimate the stress–strain internal state during the operative work. These data were used to optimize the leg, which was finally fabricated and tested, demonstrating an improvement of five times regarding the number of cycles before leg failure.

(Some figures in this article are in colour only in the electronic version)

1. Introduction

In the last few years, endoluminal devices for diagnostic and surgical applications have grown as well as established solutions for the gastrointestinal (GI) tract. Miniaturized and swallowable capsules, able to move inside the human body performing diagnosis, drug delivery and even surgical operations, represent an important achievement toward the goals of early diagnosis, minimization of patients' discomfort and health-care cost reduction [1, 2].

Commercially available wireless capsules, such as the given imaging PillCam [3], are composed by a cylindrical shell including a camera, an illumination system, electronics for image transmission and batteries. These systems move passively along the GI tract thanks to peristalsis. The main drawback of these devices is the lack of active locomotion, preventing them to stop, turn or move back during their journey. Developing active capsules would allow for exploring human body cavities in a controlled manner. A possible approach relies on external locomotion, as implemented by

Carpi *et al* [4] or Olympus [5]. These systems are steered by external magnetic fields generated outside the patient's body. An alternative solution is given by internal locomotion, for which all the motion mechanisms are embedded into the capsule. While the external approach is more effective from an energetic viewpoint, since all the power required for capsule steering is provided by the external system, internal locomotion would enable a more reliable and precise control of the capsule position and speed [6, 7].

An innovative device for the GI tract exploration adopting an internal locomotion mechanism has been developed by the authors [8, 9]. It consists of a legged endoscopic capsule (with 4, 8 or 12 legs), including one or two electromagnetic brushless motors for activating the leg sets. These legged capsules are used to obtain self-propulsion inside the intestine, and the colon in particular. Figure 1 shows three prototypes of legged robots for active capsular endoscopy, with respectively 4, 8 and 12 legs.

The main advantages of legged propulsion over other internal locomotion solutions are described in [8] and can be

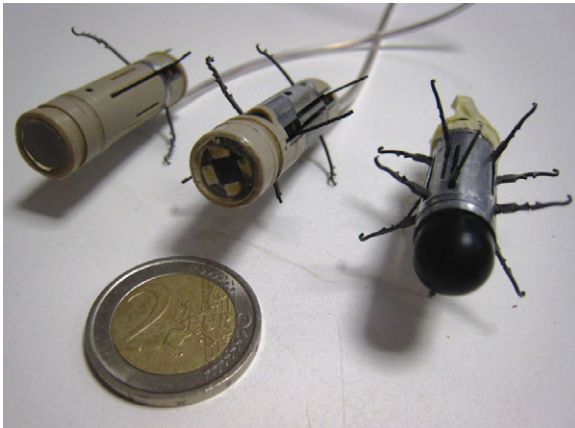


Figure 1. The three endoscopic capsule prototypes. The size ranges from 11 to 12 mm in diameter, and from 25 to 40 mm in length.

summarized as improved trajectory control, better adaptability to different diameters of the GI tract, simplified adhesion and colon wall distension, without the need of air insufflation. But a general issue that must be faced for the development of miniaturized legged devices is the leg design analysis and optimization. In fact, microfabricated legs enable capsule locomotion and represent the interface between the device and the colon walls. In order to find a trade-off between locomotion force, adaptability and tissue safety, the leg must fulfil the following requirements:

- be elastic and deformable, but at the same time strong enough to overcome tissue resistance;
- fabricated with biocompatible materials;
- guaranteeing a safe interaction with surrounding tissues.

To satisfy these requirements, Nitinol (NiTi), a titanium and nickel alloy, has been selected as the fabrication material for the capsule legs. Thanks to its superelastic properties, this material allows us to reach large deformations and to regain its original shape, once the deformation force is removed. Moreover, when a force is applied, e.g. the leg is bent by the intestine wall resistance, while the strain increases, the stress stabilizes to a plateau value. In this way the reaction force on the colon walls remains constant, thus preventing tissue injuries. Superelasticity is caused by a phase transformation between the austenitic and the martensitic phases of a crystal.

It is well known that NiTi has excellent biocompatibility and it is nowadays commonly used for a broad range of equipment in orthopaedics, neurology, cardiology and interventional radiology (e.g. Nitinol guidewires, stents, surgical clips, vena filters and clinical instruments) [10].

Regarding safety, the legged capsule was experimentally evaluated in *in vivo* porcine models [9]. During these tests the authors observed that, while the leg tips can sometimes create light red marks on the colon wall, these marks are less severe than those caused by a standard colonoscopy. On the other hand, these tests raised a very important issue related to the legs' reliability after several gait cycles. During locomotion, each leg has to withstand several bending cycles that may lead to failure and breakage: in the *in vivo* scenario, several

legs broke after an average of 35 gait cycles. This problem severely affected the locomotion reliability, since the gait was altered and became less effective due to the lack of one or more holding points for the capsule. Furthermore, 35 gait cycles are far below the requirement for a complete inspection of the colon, which needs almost 140 cycles, considering a standard colon length of 140 cm and an average distance covered by each gait of about 1 cm [9]. Therefore a design study and an optimization process for the NiTi leg are mandatory in order to reduce the failure risk and to increase the device robustness. To achieve these goals, a deep analysis and characterization of the material is required. Despite the wide commercial availability of NiTi as a structural material for smart devices, reliable data regarding its mechanical properties are not uniform in the literature. Having quantitative data, extracted from experimental trials would allow us to achieve an effective leg design through modelling and to accurately predict its behaviour. In addition to our specific application, such analysis must be considered as a general characterization of NiTi that can be applied to different devices fabricated by using this material and similar machining techniques.

In this paper, NiTi cyclic behaviour has been studied, then a FEM (finite element method) model of the leg has been developed and these data have been used to optimize the leg design, which has finally been fabricated and tested to verify the correctness of our findings.

The present paper is organized as follows. A description of the superelastic effect and an overview regarding the state of the art of NiTi mechanical characterization and modelling is reported in section 2.1. A short overview about the leg design is introduced in section 2.2, while experimental tests aimed at quantifying the cyclic behaviour of NiTi are reported in section 2.3. The analysis of NiTi cyclic behaviour is then described in section 2.4, while modelling and analysis of leg behaviour through FEM are reported in section 2.5. Finally, the leg design optimization is described in section 2.6. Section 3 discusses the performance of the new leg design after fabrication and reports the conclusions.

2. Experimental study

2.1. State of the art for NiTi mechanical properties

Figure 2 describes the typical stress–strain curve of an NiTi sample. The ‘superelastic effect’ occurs at a temperature where the material is composed of just the austenitic phase.

From an initial unloaded state, the load is increased until the austenite transforms into martensite. The phase transition spreads in the specimen under constant stress (stress plateau). The load is absorbed by the softer martensite but, as soon as the stress is decreased, the martensite begins to transform back to austenite and the specimen regain its original shape. The stress initiating the reverse transformation is denoted as σ_{AS} . Since it is lower than σ_{MF} , a hysteretic loop becomes evident in the plot.

Superelastic NiTi belongs to the larger family of shape memory alloys (SMA). Recently, the mechanical behaviour of SMAs has been studied by several groups. Bahia *et al* [11]

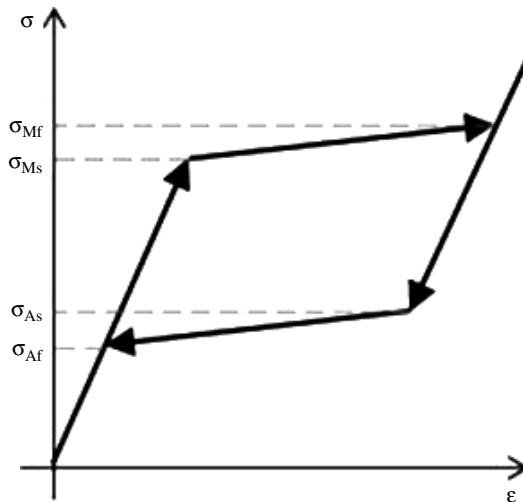


Figure 2. Schematic NiTi stress–strain curve.

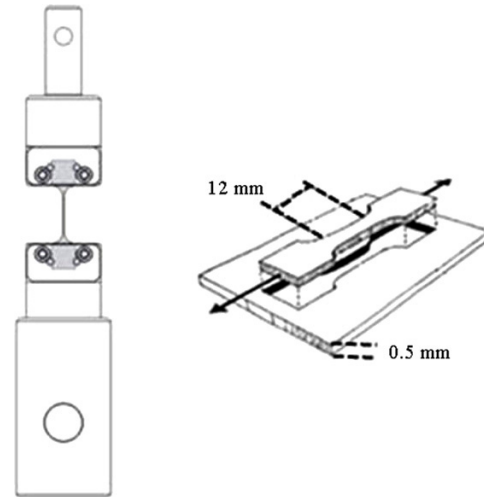


Figure 4. Set-up for the tensile tests.

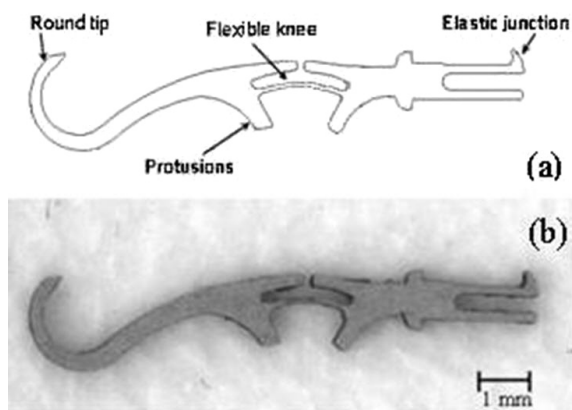


Figure 3. The preliminary leg design: (a) CAD profile, (b) fabricated leg.

analysed the influence of cyclic loading on the behaviour of NiTi wires for endodontic instruments. Tolomeo *et al* [12] quantified the cyclic deformation on superelastic Nitinol for stents, while Moumni *et al* [13] proposed a law to describe the mechanical fatigue for NiTi. Wolons [14] investigated the pseudoelastic hysteresis damping characteristics of NiTi and Ren *et al* [15] studied the hysteretic behaviour of SMAs in vibrating structures. Even if these studies are remarkable as general guidelines, small changes in nickel:titanium ratio or in the fabrication technique strongly affect the overall mechanical behaviour. For this reason, the material analysis performed in this work was based on experimental data from extensive material tests, and it can be considered as a general methodology for extracting mechanical features from superelastic materials.

2.2. Preliminary leg design

The NiTi superelastic leg was provided with a flexible joint at knee level (0.075 mm in thickness) that allowed a passive degree of freedom, as in figure 3. Thanks to this feature, the

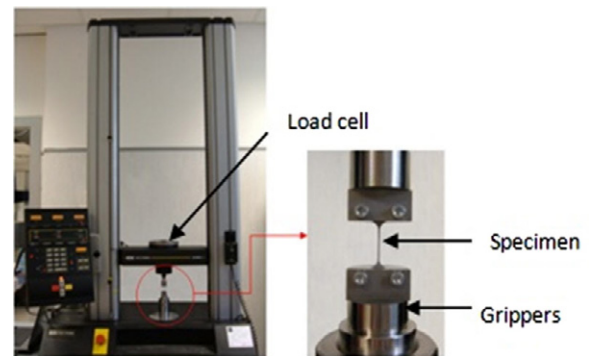


Figure 5. Experimental tensile tests.

knee was able to reach a high backwards flexure, thus adapting the locomotion to different diameters of intestinal tract and preventing tissue injuries. Furthermore, the leg was designed to bend until the two protrusions, below the knee, touch each other. A round shaped tip helped the leg to slide over the tissue. Finally, the leg was provided with an elastic junction to simplify its connection to the capsule body.

2.3. Tensile tests

In order to obtain the stress–strain curve of NiTi and its characteristic parameters (Young's modulus, typical stresses, residual deformation), extensive tensile tests were carried out.

The tests were performed using an electromechanical universal dual-column testing machine (4464, Instron, USA) with a load cell having a range of 1.0 kN. The data were acquired by a computer-based data acquisition system through purposely developed software. The experimental set-up is shown in figures 4 and 5.

The material under test was the same used to fabricate the legs and was machined by the same method. In particular, the SMA specimen was cut from an NiTi sheet (*Alloy S-Superelastic standard alloy*, Memory-Metalle GmbH, Germany) by μ wire electrical discharge machining (AP 200L,

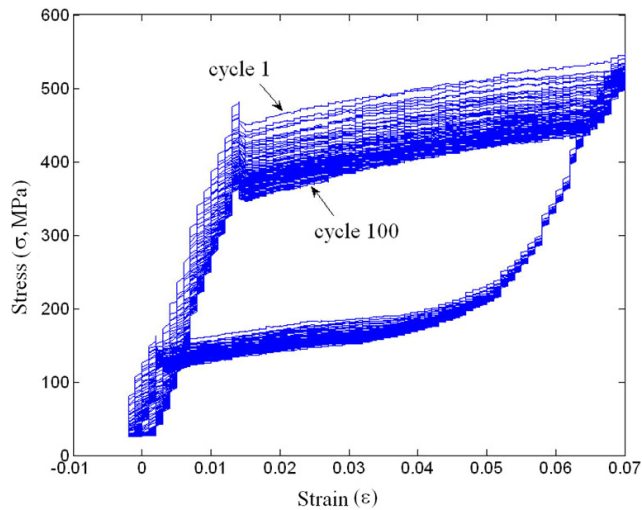


Figure 6. Experimental stress–strain curve for 100 loading–unloading cycles.

Sodick, Japan). Alloy *S* was chosen for its superelastic properties. The atomic compositional average is around 50.8% in Ni and the austenitic finish temperature is 0°C, thus guaranteeing a superelastic behaviour at room temperature. The shape of the specimen was optimized by FEM simulations in order to adapt the stress values to the measurement range of the load cell. The specimen thickness was the same in the leg (0.5 mm). Two purposely designed steel grippers, also shown in figure 4, were used to hold it and to prevent both slippage and stress concentration.

Regarding loading settings, the tests were performed in isothermal conditions (room temperature) under displacement control. The maximum recovery strain of NiTi is about 8%; therefore the maximum strain in the tests was selected as 7% to induce complete austenite–martensite transformation without reaching the material yield point (750 MPa).

Initially, the unloaded specimen presented an austenitic microstructure. It was pre-stressed to a level between 20 and 30 MPa to ensure a firm hold on the grippers. A displacement of 0.42 mm was imposed, corresponding to a 7% deformation, at a constant speed of 0.75 mm min⁻¹. Then the system was carried back to zero-load condition.

In order to observe the cyclic behaviour of the material, 100 loading/unloading cycles were performed, at an acquisition rate of 10 samples s⁻¹. Such a number of cycles would guarantee the reliability of results, as further explained in section 2.4.

2.4. Cyclic behaviour of NiTi

During the tests, stress–strain values were recorded.

In the stress–strain curve, shown in figure 6, the characteristic behaviour of SMAs is clearly visible. In particular, the trend of the curve changes as the number of cycles increases.

- The stress σ_{Ms} , which marks the beginning of the plateau, drops significantly due to internal stresses which reduce

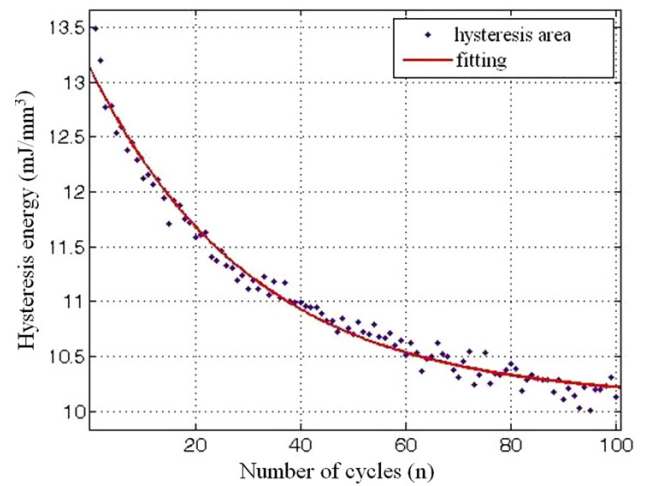


Figure 7. Hysteresis energy versus number of cycles curve.

the effort required to change the phase. The material is experiencing a kind of cyclic softening, becoming gradually less rigid in accordance with [12, 16].

- The lower plateau undergoes a significantly smaller change: this leads to a reduction in the hysteretic loop, then a decrease of the dissipated energy per cycle. This variation stabilizes with cycles; these results agree with those of [13, 16].
- The residual deformation in zero-load conditions increases significantly during the first few cycles due to the accumulation of internal deformation, as also highlighted in [11, 13].

In order to establish if, after 100 iterations, the hysteretic behaviour could be considered stable, the ‘hysteresis energy versus number of cycles’ curve was traced. The hysteresis energy is defined as the dissipated energy per unit volume in each loading–unloading cycle, and it corresponds to the loop surface area (figure 7).

The curve follows an exponential law:

$$y = ae^{(-bn)} + c. \quad (1)$$

After an initial sharp slope, it stabilized asymptotically. The data were analysed through the Matlab software. The fitting procedure, applied to experimental data, gave the following parameters:

- $a = 3.021 \text{ mJ mm}^{-3}$;
- $b = 0.03243$;
- $c = 10.11 \text{ mJ mm}^{-3}$ (energy plateau).

The percentage error between the cycle n energy and the energy plateau c is

$$\text{err}(n) = \left(\frac{y(n) - c}{c} \right) 100. \quad (2)$$

For the 100th cycle curve, $\text{err}_{(100)}$ was 1.17%. For this reason, the 100th curve could be considered stable, and it was chosen to extract the parameters used for the FEM analysis, as described in section 2.5.

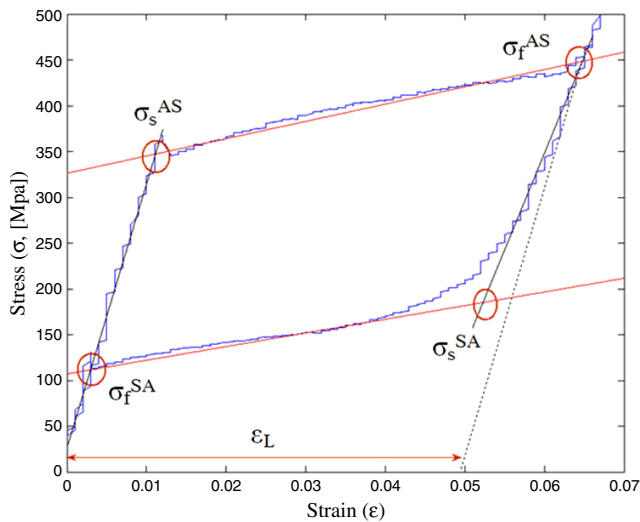


Figure 8. The 100th cycle curve with constants highlighted.

2.5. FEM analysis

In order to predict the leg behaviour during locomotion in the colon, a FEM model was developed with ANSYS 10.0.

As a first step, a FEM analysis of the tensile test was carried out to evaluate simulation reliability. The results were compared with the experimental evidence, to highlight the differences in behaviour between the model and the real sample. The ANSYS option SMA, which allows simulating the nonlinear behaviour of NiTi, was adopted. This option describes a combination of elastic–plastic behaviour, defined by five constants [17]. The data previously obtained from tensile tests were used as input for the FEM analysis. In particular, the five constants were extracted from the 100th cycle, which was assumed to describe the stabilized behaviour of the material.

Thus, as represented in figure 8, the following values were chosen:

- $E = 27575$ as the Young's modulus;
- $\sigma_s^{AS} = 339$ MPa as the starting stress value for the forward phase transformation (austenite–martensite);
- $\sigma_f^{AS} = 440.95$ MPa as the final stress value for the forward phase transformation (austenite–martensite);
- $\sigma_s^{SA} = 185.5$ MPa as the starting stress value for the reverse phase transformation (martensite–austenite);
- $\sigma_f^{SA} = 112.6$ MPa as the final stress value for the reverse phase transformation (martensite–austenite);
- $\varepsilon_L = 0.048$ as the residual deformation.

A quarter of the specimen was modelled, taking advantage of its symmetry properties. The same displacement of the tensile tests (0.42 mm) was applied in the simulation. A 3D model was used, *SOLID 186* was chosen as the element and the load was applied gradually by means of several *load steps*. The simulation results for von Mises' stress and total strain are shown in figure 9.

As regard the strain, the maximum value of 6.24% was achieved in the central narrowing, while the rest of the specimen had a negligible strain.

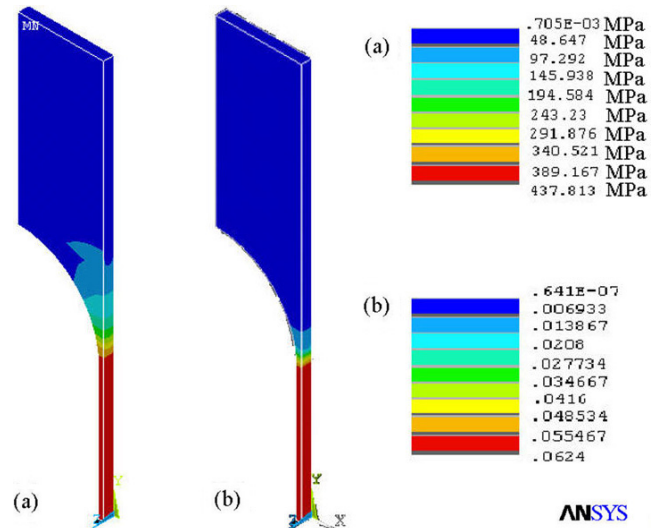


Figure 9. FEM simulation results for tensile tests. (a) Von Mises' stress, (b) total strain.

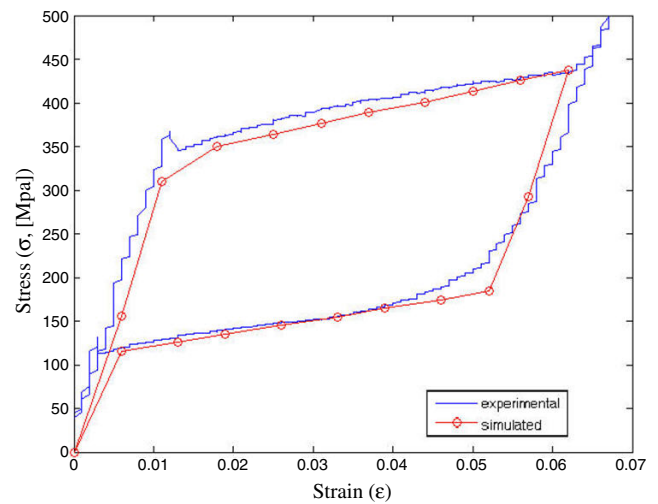


Figure 10. Curves from experimental test (solid) and from simulated model (dotted).

Concerning the von Mises stress, it was concentrated uniformly in the central area, reaching a maximum value of 437.8 MPa.

The stress–strain values, extracted from the simulation steps of the 100th cycle, are shown in figure 10 (dotted line) and compared with experimental data (solid line). From these results it is possible to assume that the developed FEM model was consistent with the experimental test.

To further confirm this assumption, the two hysteresis surface areas were evaluated as 10.75 mJ mm^{-3} for the experimental curve and 11.72 mJ mm^{-3} for the simulation values, thus resulting in an acceptable 9% relative error.

2.6. Leg design optimization

In order to infer about leg behaviour and to work towards design optimization to prevent failure, the leg geometry was

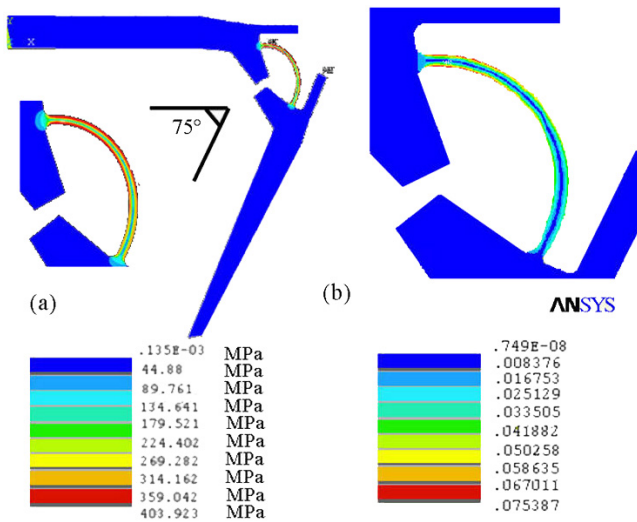


Figure 11. FEM simulation of the bended leg. (a) Von Mises' stress, (b) total strain in the knee.

modelled. Given the peculiar geometry of the leg, a 2D model was considered a proper schematization. In fact, we experimentally observed that the leg deformation usually occurs in a plane parallel to the leg surface. Particular care was devoted to the flexible knee, since this was the weakest area. This section must withstand nearly the total leg deformation, while experiencing stress intensification due to the localized necking. Therefore, a 2D model was developed by using ANSYS analysis for large deformations and plane strain options (deformation in the normal plane was assumed to be negligible). The geometry was designed in terms of parameters (through ANSYS Parametric Design Language), enabling iterative modifications of the knee shape.

The ranges of applied loads and displacements were chosen as in the operative scenario:

- the leg base was constrained, since this part is usually fixed to the capsule body;
- a displacement of 7.5 mm was applied on the leg tip, simulating the movement derived from interactions with the intestinal wall;
- the joint was flexed to an angle of 75°.

From simulation results, reported in figure 11, it was possible to extract typical stress and strain values occurring in the leg knee during capsule locomotion.

The maximum stress value was 403.9 MPa, achieved in the knee, withstanding a composed solicitation of bending and cutting. The lateral fibres of the knee were the most loaded areas, since these external and internal regions were subjected, respectively, to tension and compression during bending. Furthermore, the strain was also concentrated in the flexible knee, while the rest of the structure was virtually rigid. In the external fibres a strain of 7.5% was achieved.

As a validation of the FEM analysis reliability, it is important to underline that this area is the same that, during operative work, failed more frequently, as demonstrated in figure 12.

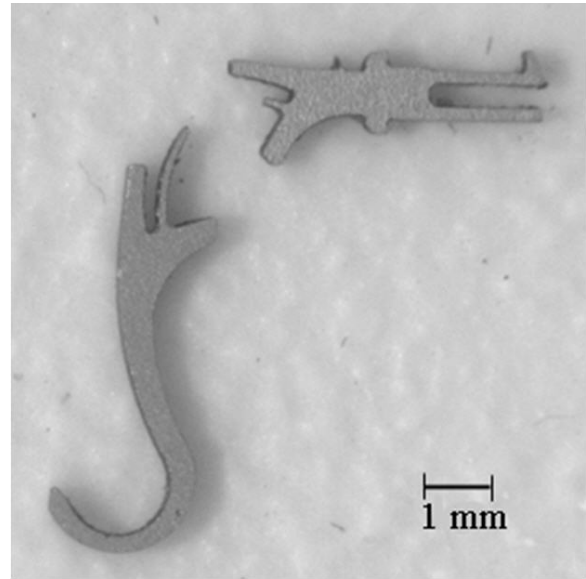


Figure 12. A broken leg after repeated operative cycles.

The maximum stress value obtained by simulations was still on the superelastic plateau, even if very close to σ_{Mf} . The strain peak value was lower than the maximum recovery strain (8%), but still very close to this value.

These conditions led to a very high risk of overcoming threshold values, thus resulting in leg failure. In order to reduce such risk, the leg geometry was modified iteratively and the developed finite element model was used to predict the expected stresses in the modified designs.

It is important to highlight that such an optimization process was mainly driven by technological issues. Therefore, the variable design parameters were chosen within a limited number of solutions that were feasible in terms of manufacturability. Moreover, the leg design must respect some predetermined dimensional constraints in order to properly fit with the capsule body.

The main goal for this design optimization process was to reduce the maximum stress value.

The knee can be modelled as a beam subjected to bending, where the maximum stress can be expressed as

$$\sigma_{\max} = \left(\frac{3Eh}{l^2} \right) F_{\max} \quad (3)$$

where F_{\max} is the force required at leg tip to open a collapsed tissue, l and h are the knee length and the thickness, respectively.

Since F_{\max} is usually assumed to be 0.25 N [8], a reduction of σ_{\max} must be achieved by modifying l and h . Thus l was increased and h was reduced. In particular, h was assumed as a function of a longitudinal variable x :

$$h(x) = h_0 - \alpha x \quad (4)$$

where $h_0 = 0.08$ mm is the knee thickness in the initial part, as reported in figure 13.

The parameter α was obtained first by fixing the maximum and minimum values for h (between 0.08 and 0.06 mm), which

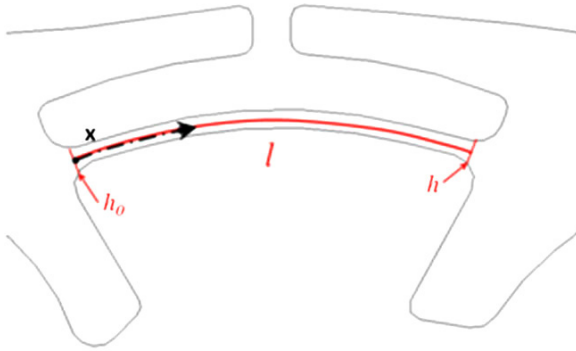


Figure 13. Knee geometry.

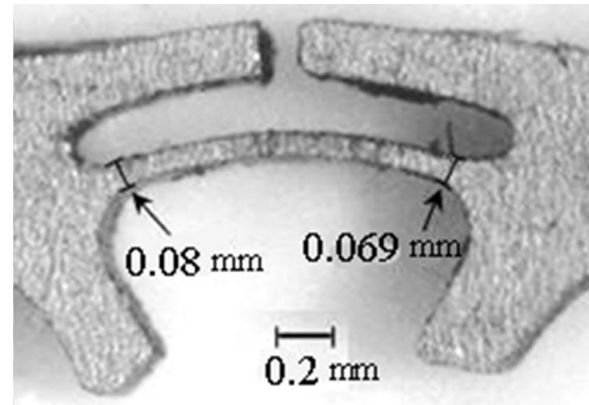


Figure 14. Detail of the optimized knee design.

Table 1. Dimensional parameters for the leg design.

	h_0 (mm)	h (mm)	l (mm)
Preliminary design	0.075	0.075	1.54
Optimized design	0.08	$h_0 - 0.006x$	1.81

were mainly imposed by fabrication limits. Then, several values for α were implemented in the finite element model, ranging from 0.001 to 0.01, in order both to achieve the most uniform stress distribution and to find the best trade-off between reduction in h dimensions and a smooth thickness decrease. This procedure led to a final value for α of 0.006. This solution guaranteed a linear decrease in thickness along the longitudinal direction, thus allowing a more regular stress distribution.

The total knee length l was fixed at 1.81 mm. This value resulted from an iterative process. Several FEM simulations were carried out with different l values, ranging from the preliminary size (1.54 mm) to $l = 2$ mm, imposed by fabrication constraints. The chosen value enabled a reduction in the stresses and allowed us to obtain the most uniform stress distribution among the tested values.

The dimensional parameters for the preliminary and the optimized design are reported in table 1.

The FEM stress distribution for the optimized design is represented in figure 14. Thanks to this optimization process, a 10% reduction of the maximum stress value was achieved by the novel design, where $\sigma_{\max} = 360$ MPa. This value still falls in the superelastic plateau, thus allowing the phase change. Moreover, the strain is maintained at less than 3%. These results reduced the chances to lose the superelastic properties after repeated cycles and therefore the risk of leg failure.

The novel leg design (figure 15) was experimentally tested, achieving an average value of 150 cycles before leg failure, thus enabling a safe and effective active exploration of the entire colon.

3. Conclusions

This work originated from the optimization need of a superelastic leg for an endoscopic capsule, and it presents an experimental study on Nitinol and an example of FEM tuning and simulation for this material.

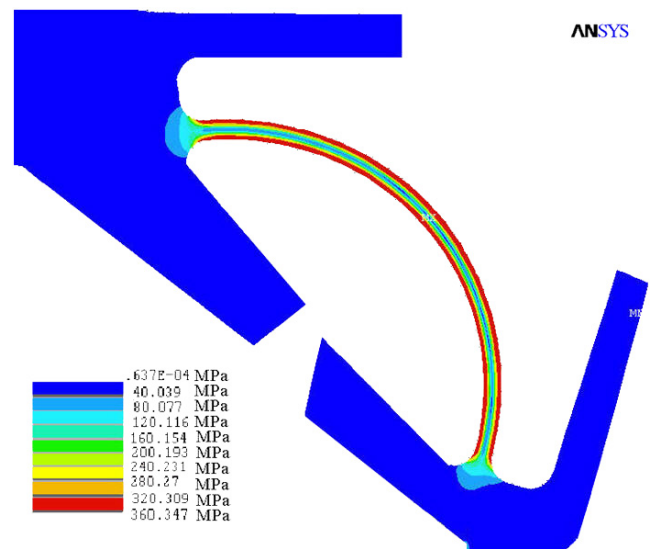


Figure 15. FEM stress distribution for the optimized design.

The approach to design optimization of superelastic structures illustrated in the present paper can be a useful guideline for different Nitinol structures.

First, the NiTi stress-strain curve measurement and the analysis of the mechanical cycles were performed in order to have a solid base for the further development of our work. The hysteresis energy was calculated and 100 iterations were found to be a satisfying threshold for stable behaviour. Then, a rigorous procedure for approaching the design of superelastic hinges with the aid of FEM-based software was developed. The experimental results have been used to set the internal parameters of a FEM model for the superelastic leg. This allowed us to obtain a reliable and useful simulation platform for leg design optimization. The final design was finally fabricated and tested, achieving performances five times better than the previous ones in terms of average number of cycles before leg failure.

Further improvements in leg lifetime can be obtained by using a different kind of machining. The fabrication method influences critically the knee surfaces: in fact, wire electrical discharge machining produces defects and cracks that

propagate easily through the very thin thickness of the material. A solution could be to apply an electro-polishing procedure to enhance superficial resistance to cracks.

Starting from this work, another important improvement could be setting up fatigue bending tests. This would enable a precise prediction of both the fatigue behaviour and the lifetime of the material under cyclic bending solicitations. This is a complex issue, due to the peculiar behaviour of NiTi, but it could represent a further step to enhance the leg design optimization.

Acknowledgments

This work was supported in part by the Intelligent Microsystem Center, Korea Institute of Science and Technology (KIST), Korea, in part by the European Commission in the framework of the VECTOR FP6 European Project and by the Italian Institute of Technologies (IIT).

The authors are also grateful to N Funaro and G Favati for the manufacturing of prototypes and C Quaglia for his invaluable help.

References

- [1] Moglia A, Menciassi A and Dario P 2008 Recent patents on wireless capsule endoscopy *Recent Pat. Biomed. Eng.* **1** 24–33
- [2] Gay G, Delvaux M and Rey J F 2004 The role of video capsule endoscopy in the diagnosis of digestive diseases: a review of current possibilities *Endoscopy* **36** 913–20
- [3] <http://www.givenimaging.com>
- [4] Carpi F, Galbiati S and Carpi A 2007 Controlled navigation of endoscopic capsules: concept and preliminary experimental investigations *IEEE Trans. Biomed. Eng.* **54** 2028–36
- [5] <http://www.olympus.co.jp>
- [6] Menciassi A, Quirini M and Dario P 2007 Microrobotics for future gastrointestinal endoscopy *Minim. Invasive Ther. Allied Technol.* **16** 91–100
- [7] Park H, Park S, Yoon E, Kim B, Park J and Park S 2007 Paddling based microrobot for capsule endoscopes *IEEE Int. Conf. on Robotics and Automation (Roma)* pp 3377–82
- [8] Quirini M, Menciassi A, Scapellato S, Stefanini C and Dario P 2008 Design and fabrication of a motor legged capsule for the active exploration of the gastrointestinal tract *IEEE/ASME Trans. Mechatron.* **13** 169–79
- [9] Quirini M, Scapellato S, Menciassi A, Dario P, Rieber F, Ho C N, Schostek S and Schurr M O 2008 Feasibility proof of a legged locomotion capsule for the gastrointestinal tract *Gastrointest. Endosc.* **67** 1153–58
- [10] Morgan N B 2004 Medical shape memory alloy applications—the market and its product *Mater. Sci. Eng. A* **378** 16–23
- [11] Bahia M G A, Gonzalez B M and Buono V T L 2006 Fatigue behaviour of nickel-titanium superelastic wires and endodontic instruments *Fatigue Fract. Eng. Mater. Struct.* **29** 518–23
- [12] Tolomeo D, Davidson S and Santinoranont M 2001 Cyclic properties of superelastic Nitinol: design implications *SMST-2000 Conf. Proc.* pp 471–76
- [13] Moumni Z, Van Herpen A and Riberty P 2005 Fatigue analysis of shape memory alloys: energy approach *Smart Mater. Struct.* **14** S287–92
- [14] Wolons D, Gandhi F and Malovrh B 1998 Experimental investigation of the pseudoelastic hysteresis damping characteristics of shape memory alloy wires *J. Intell. Mater. Syst. Struct.* **9** 116–26
- [15] Ren W, Li H and Song G 2007 Phenomenological modeling of the cyclic behavior of superelastic shape memory alloys *Smart Mater. Struct.* **16** 1083–89
- [16] Lim T J and Mc Dowell D L 1995 Path dependence of shape memory alloys during cyclic loading *J. Intell. Mater. Syst. Struct.* **6** 817–30
- [17] ANSYS Inc. 2005 Theory reference ANSYS release 10.0 chapter 4, section 6, p 41